Neuroscience 340 (2017) 48–61

α4β2* NICOTINIC RECEPTORS STIMULATE GABA RELEASE ONTO FAST-SPIKING CELLS IN LAYER V OF MOUSE PREFRONTAL (Fr2) CORTEX

PATRIZIA ARACRI,[a†] SIMONE MENEGHINI,[a†] AURORA COATTI,[a] ALIDA AMADEO[b] AND ANDREA BECCHETTI[a*]

[a] *Department of Biotechnology and Biosciences, and NeuroMI (Milan Center of Neuroscience), University of Milano-Bicocca, piazza della Scienza 2, Milano 20126, Italy*

[b] *Department of Biosciences, University of Milano, Via Celoria 26, Milano 20133, Italy*

Abstract—Nicotinic acetylcholine receptors (nAChRs) produce widespread and complex effects on neocortex excitability. We studied how heteromeric nAChRs regulate inhibitory post-synaptic currents (IPSCs), in fast-spiking (FS) layer V neurons of the mouse frontal area 2 (Fr2). In the presence of blockers of ionotropic glutamate receptors, tonic application of 10 μM nicotine augmented the spontaneous IPSC frequency, with minor alterations of amplitudes and kinetics. These effects were studied since the 3rd postnatal week, and persisted throughout the first two months of postnatal life. The action of nicotine was blocked by 1 μM dihydro-β-erythroidine (DHβE; specific for α4* nAChRs), but not 10 nM methyllycaconitine (MLA; specific for α7* nAChRs). It was mimicked by 10 nM 5-iodo-3-[2(S)-azetidinyl methoxy]pyridine (5-IA; which activates β2* nAChRs). Similar results were obtained on miniature IPSCs (mIPSCs). Moreover, during the first five postnatal weeks, approximately 50% of FS cells displayed DHβE-sensitive whole-cell nicotinic currents. This percentage decreased to ~5% in mice older than P45. By confocal microscopy, the α4 nAChR subunit was immunocytochemically identified on interneurons expressing either parvalbumin (PV), which mainly labels FS cells, or somatostatin (SOM), which labels the other major interneuron population in layer V. GABAergic terminals expressing α4 were observed to be juxtaposed to PV-positive (PV+) cells. A fraction of these terminals displayed PV immunoreactivity. We conclude that α4β2* nAChRs can produce sustained regulation of FS cells in Fr2 layer V. The effect presents a presynaptic component, whereas the somatic regulation decreases with age. These mechanisms may contribute to the nAChR-dependent stimulation of excitability during cognitive tasks as well as to the hyperexcitability caused by hyperfunctional heteromeric nAChRs in sleep-related epilepsy.

Key words: heteromeric nAChR, interneuron, IPSC, parvalbumin, PFC, somatostatin.

INTRODUCTION

In the neocortex, acetylcholine (ACh) regulates arousal and executive functions (Jones, 2008), and the implication of nAChRs is increasingly recognized (Wallace and Bertrand, 2013). The main nAChR subtypes are the low-affinity and quickly desensitizing homopentamer (α7)5 and the high-affinity and slowly desensitizing heteropentamer α4β2*. Both regulate cognitive processes, although their specific roles and the contribution of other subunits are debated (Albuquerque et al., 2009; Parikh et al., 2010; Guillem et al., 2011; Picciotto et al., 2012; Bloem et al., 2014; Zoli et al., 2015). In general, the kinetic and pharmacological features of heteromeric nAChRs make them particularly fit to regulate overall excitability, particularly on a relatively slow time scale, as is likely to occur during non-synaptic, diffuse transmission (Lendvai and Vizi, 2008). This concept agrees with the observation that mutant α4 and β2 subunits are frequently linked to ADNFLE (autosomal dominant nocturnal frontal lobe epilepsy, Becchetti et al., 2015).

In rodents, heteromeric nAChRs regulate excitatory as well as inhibitory neurons in medial (Lambe et al., 2003; Couey et al., 2007; Kassam et al., 2008; Zolles et al., 2009) and dorsomedial (Aracri et al., 2010, 2013) prefrontal cortex (PFC). Moreover, functional heteromeric nAChRs are observed in GABAergic interneurons dissociated from surgical samples from human neocortex (Alkondon et al., 2000). However, how nAChRs expressed in different compartments interplay in prefrontal circuits is unclear. In particular, the nicotinic modulation of distinct interneuron classes is poorly understood, despite the notorious sensitivity of neocortical

*Corresponding author. Address: Department of Biotechnology and Biosciences, University of Milano-Bicocca, piazza della Scienza, 2. Milano 20126, Italy. Fax: +39-02-64483565.

E-mail address: andrea.becchetti@unimib.it (A. Becchetti).

† These authors contributed equally to the paper.

Abbreviations: 5-IA, 5-iodo-3-[2(S)-azetidinylmethoxy]pyridine; ACh, acetylcholine; ADNFLE, autosomal dominant nocturnal frontal lobe epilepsy; AHP, after-hyperpolarization; AP, action potential; AP5, D(−)-2-amino-5-phosphono-pentanoic acid; BSA, bovine serum albumin; CNQX, 6-cyano-7-nitroquinoxaline-2,3-dione; DF, degrees of freedom; DHβE, dihydro-β-erythroidine; Fr2, frontal area 2; FS, fast-spiking; IPSC, inhibitory postsynaptic current; KS, Kolmogorov–Smirnov; mIPSC, miniature IPSC; MLA, methyllycaconitine; nAChR, nicotinic acetylcholine receptor; NS, not significantly different; PBS, phosphate buffered saline; PFC, prefrontal cortex; PV, parvalbumin; R_{in}, input resistance; SOM, somatostatin; TTX, tetrodotoxin; VGAT, vesicular GABA transporter; V_{rest}, resting membrane potential.

http://dx.doi.org/10.1016/j.neuroscience.2016.10.045

excitability to the GABAergic tone (Isaacson and Scanziani, 2011). Another source of uncertainty is the increasing recognition that different PFC regions present heterogeneous structures and connectivities (Franklin and Chudasama, 2012). Hence, nAChRs may exert different roles in different areas.

We studied the dorsomedial shoulder region of murine PFC, or frontal area 2 (Fr2), which bears relation to the dorsolateral PFC in humans (Uylings et al., 2003). This region innervates the motor cortex and the dorsolateral striatum and receives afferents from sensory and parietal cortices as well as ventral tegmental dopamine neurons (Berendse et al., 1992; Condé et al., 1995). Hence, Fr2 appears to be a pivotal target of cholinergic transmission, as in rodents it mediates the decision and execution steps preceding the motivation-dependent purposeful tasks, particularly those requiring immediate attention (Kargo et al., 2007). Moreover, because Fr2 is connected with both motor cortex and striatum, the nicotinic regulation of excitability in this region may be particularly relevant in the development of ADNFLE seizures, which are typically accompanied by hypermotor seizures and the release of stereotyped motor patterns (Becchetti et al., 2015).

We here focus on the regulation of FS cells by heteromeric nAChRs in Fr2 layer V. The latter layer constitutes the main output channel to subcortical structures and is crucial for spread of synchronized activity (Richardson et al., 2008). Pyramidal neurons in layer V are tightly controlled by a dense network of GABAergic cells (Shu et al., 2003; Ozeki et al., 2009), and FS cells are especially implicated in feed-forward inhibition (Cammarota et al., 2013). Moreover, FS neurons are major regulators of neocortical output during cognitive operations, and drive network oscillations at different frequencies (Cardin et al., 2009; Sohal et al., 2009). Inhibitory interneurons are known to be connected by reciprocal as well as autaptic GABAergic synapses, and such evidence is particularly ample in sensory cortices (Tamás et al., 1997; Galarreta and Hestrin, 2002; Bacci et al., 2003; Jiang et al., 2013). Disinhibition of local interneurons is implicated in regulating visual signal elaboration (Pfeffer et al., 2013), auditory discrimination (Pi et al., 2013), learning in auditory cortex (Letzkus et al., 2011).

In general, circuit disinhibition may be a widespread mechanism contributing to different aspects of learning (Letzkus et al., 2015) and cognition (Murray et al., 2014). However, scarce information is available about how neurotransmitters shape reciprocal inhibition between interneurons in PFC, and virtually nothing is known about these mechanisms in associative areas. We show that, in layer V, $\alpha4\beta2^*$ nAChRs regulate GABA release onto FS neurons. The effect was studied since the third postnatal week, a phase of neocortex maturation and modification of nAChR expression, and was maintained at least until the end of the second postnatal month, when the neocortical circuits have reached maturity and the nAChR expression is stable (Molas and Dierssen, 2014). These results reveal a supplementary mechanism to stimulate physiological excitability as well as a possible cause of pathological hyperexcitability in prefrontal regions.

EXPERIMENTAL PROCEDURES

Drugs and chemicals

We purchased chemicals from Sigma–Aldrich (Milan, Italy), except D(−)-2-amino-5-phosphono-pentanoic acid (AP5), 6-cyano-7-nitroquinoxaline-2,3-dione (CNQX), tetrodotoxin (TTX) and 5-iodo-3-[2(S)-azetidinylmethoxy] pyridine (5-IA) (Tocris Bioscience, Bristol, UK). AP5, TTX citrate, (−)-nicotine hydrogen tartrate salt, (−)-bicuculline methiodide, MLA citrate hydrate, and DHβE hydrobromide were dissolved in distilled water, and stored at −20 °C. Stock solutions of CNQX were prepared in dimethylsulfoxide (20 mM). Stock solutions of 5-IA were prepared in our extracellular solution, and diluted daily as necessary.

Brain slices

We used FVB mice of both sexes (Harlan Laboratories Srl, Lesmo, Italy), as previously described (Aracri et al., 2013). Our procedures followed the Principles of Laboratory Animal Care (86/609/EEC Directive of 1986), and were approved by the Italian Ministry of Health. In brief, Fr2 coronal sections were cut between +2.68 mm and +2.10 mm from bregma. A sketch is shown in Fig. 1A. For patch-clamp experiments, brains were extracted from P16–P63 mice (n = 53) after isoflurane anesthesia, and placed in the following ice-cold solution (mM): 87 NaCl, 21 $NaHCO_3$, 7 $MgCl_2$, 1.25 NaH_2PO_4, 0.5 $CaCl_2$, 2.5 KCl, 75 sucrose, 25 D-glucose, 400 μM ascorbic acid, and bubbled with 95% O_2 and 5% CO_2 (pH 7.4). Slices (300 μm thick) were prepared and maintained as previously described (Aracri et al., 2013). For immunocytochemistry, mice (P19–P90; n = 9) were anesthetized with intraperitoneal 2 mg/100 g chloral hydrate, after isoflurane pre-anesthesia, and sections (50 μm thick) were prepared as previously described (Aracri et al., 2010).

Whole-cell recording

Experiments were carried out under a direct microscope (Eclipse E600FN), equipped with differential interference contrast (DIC) water immersion objective (Nikon Instruments, Milan, Italy), and an infrared digital CCD C8484-05G01 camera, equipped with HCImage Live acquisition software (Hamamatsu Photonics Italia, Arese, Italia). Stimulation and recording were performed with a Multiclamp 700A (Molecular Devices, Sunnyvale, CA), at 33–34 °C. Patch-clamp pipettes (2–3 MΩ) were pulled with a P-97 Micropipette Puller (Sutter Instruments, Novato, CA), from borosilicate capillaries (Corning Inc., NY, USA) with an inside and outside diameter of 0.86 mm and 1.5 mm, respectively. We always compensated the series resistance (up to approximately 75%) and cell capacitance. The former was generally below 10 MΩ. Current traces were filtered at 2 kHz (low-pass) and digitized at 5 kHz, with Molecular Devices hardware and software (pClamp9/Digidata 1322A). Slices were perfused (~2 ml/min) with artificial cerebrospinal fluid, containing (mM): 135 NaCl, 21 $NaHCO_3$, 0.6 $CaCl_2$, 3 KCl, 1.25 NaH_2PO_4, 1.8

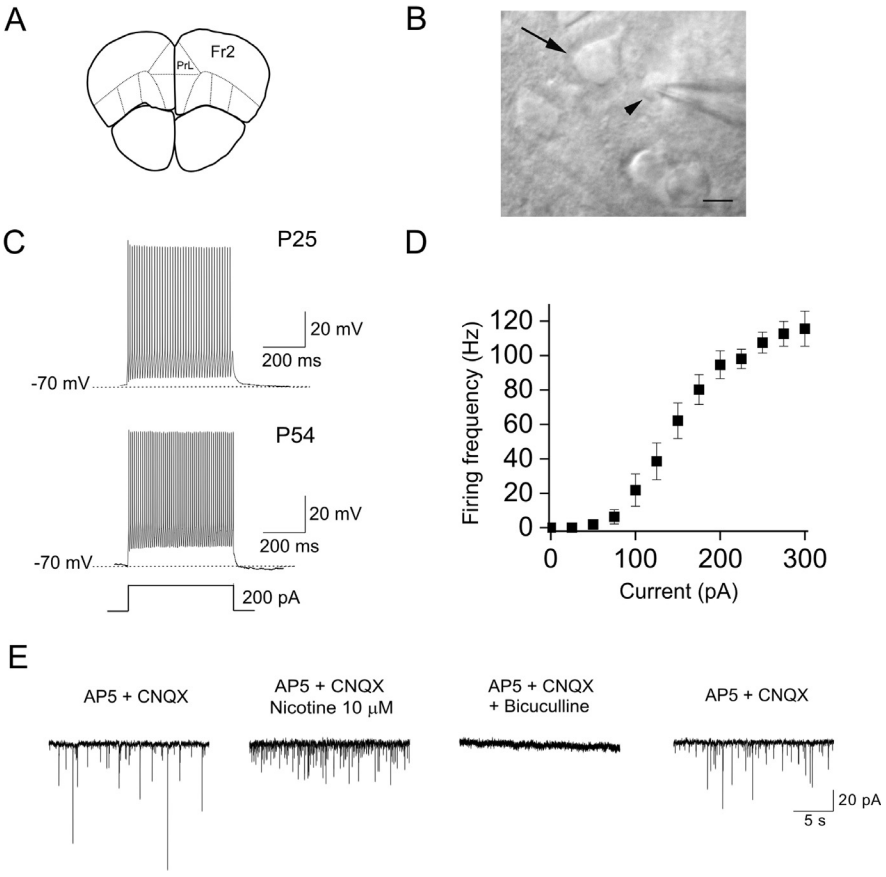

Fig. 1. FS cells in Fr2 layer V. (A) Schematic of a coronal murine PFC section, representing the frontoparietal region between +2.68 and +2.10 mm from bregma. Based on Paxinos and Franklin (2001). PrL: prelimbic; Fr2: frontal area 2. (B) Micrograph of a FS cells under recording (arrowhead), adjacent to a pyramidal neuron (arrow). Scale bar = 10 μM. (C) Firing response to a 200-pA depolarizing currents, in FS cells from mice of different ages. (D) Average frequency–stimulus relation for a representative sample of FS cells. (E) IPSC traces, at −70 mV, in the indicated conditions. In this representative experiment, all synaptic events were abolished by bicuculline.

$MgSO_4$, 10 D-glucose, aerated with 95% O_2 and 5% CO_2 (pH 7.4). Pipette was filled with (mM): 70 K-gluconate, 70 KCl, 2 $MgCl_2$, 0.5 BAPTA, 1 MgATP, 10 HEPES (pH 7.2). For the experiments at physiological intracellular Cl^- concentration, we used 135 K-gluconate and 5 KCl, leaving the other concentrations unchanged. V_{rest} (resting potential) was measured soon after obtaining the whole-cell configuration. Input resistance was measured by applying small stimuli around V_{rest}. No correction was applied for liquid junction potentials. Drugs were applied in the bath, and the maximal effect was usually reached within ~2 min. Only one experiment was carried out in each slice, to avoid uncontrolled long-term effects of nicotinic agonists (e.g., on nAChR desensitization).

Analysis of patch-clamp data

Action potentials (APs) and inhibitory post-synaptic currents (IPSCs) were analyzed off-line by using Clampfit 9.2 (Molecular Devices), and OriginPro 9.1 (OriginLab Corporation, Northampton, MA, USA). In Table 1, spike width was calculated at half-amplitude, and spike amplitude was computed as the difference between the AP threshold and the peak. Spike intervals were measured between consecutive peaks. Adaptation was measured at a firing frequency of ~100 Hz (average-spiking frequency in the stimulus time). After-hyperpolarization (AHP) was measured as the difference between the AP threshold and the most negative V_m reached on repolarization. IPSCs included smooth isolated signals as well as composite signals. Individual IPSCs were inspected to reject spurious events. The baseline noise (peak-to-peak) was generally ~5 pA. Because the minimal IPSC amplitude was expected to be around 5 pA (Ghosh et al., 2015), we set the detection threshold at 5–6 pA. The effect of treatments (or recovery) was usually measured for 2 min after reaching the maximal effect. After washout, IPSC frequency was usually larger than 70% of the initial value. Cells in which this value was lesser than 50% were discarded. IPSC kinetics were analyzed on 50 single events per cell, in the absence or presence of nicotine. IPSC decay was fitted with a standard monoexponential function (Léna and Changeux, 1997).

Sections for confocal microscopy

For immunocytochemistry, sections were treated as previously described (Aracri et al., 2013). Image analysis was carried out with a TCS SP2 AOBS confocal microscope (Leica Microsystems). To test the specificity of immunoreaction, negative controls were performed by omitting primary antibodies.

Primary antibodies

Polyclonal anti-α4 nAChR: made in guinea pig, diluted at 1/1000 (Millipore, Milan, Italy). Polyclonal anti-Vesicular GABA transporter (VGAT): made in rabbit, 1/1500 (Synaptic Systems, Goettingen, Germany). Polyclonal anti-PV: made in rabbit, 1/2000 (SWant Inc., Marly, Switzerland). Monoclonal anti-PV: made in mouse, 1/1000 (Sigma–Aldrich). Monoclonal anti-somatostatin (anti-SOM): made in rat, 1/300 (Millipore).

Secondary antibodies

For α4 nAChR: biotinylated anti-guinea pig IgG, made in donkey (bDAGp; 1/200; Vector Laboratories, CA), and Alexa-488-labeled streptavidin (1/200; Molecular

Table 1. Electrophysiological features of FS cells, during the first two postnatal months

Age (week)	V_{rest} (mV)	Spike width (ms)	4th spike interval/1st spike interval	AHP (mV)	*N*
3rd	−69.3 ± 0.45	0.70 ± 0.06	1.36 ± 0.06	−13.6 ± 1.6	13
4th	−70.1 ± 0.25	0.71 ± 0.05	1.27 ± 0.05	−14.5 ± 0.9	28
5th	−69.6 ± 1.26	0.90 ± 0.16	1.33 ± 0.09	−13.7 ± 3.2	5
7th–9th	−70.0 ± 0.65	0.75 ± 0.16	1.13 ± 0.04	−11.7 ± 0.7	23

Firing parameters at the indicated postnatal weeks. For comparison, the ratios between the fourth and the first spike interval in a sample of pyramidal cells from the same mice were 2.3 ± 0.48 (< P28; $n = 9$), and 2.6 ± 0.39 (> P28; $n = 14$), at firing frequencies of 10–50 Hz. All differences between age groups were NS. In a representative sample of FS cells ($n = 8$, from six mice) R_{in} was 82.2 ± 7 MΩ in the first month, and 55.6 ± 4.5 MΩ after P45 ($n = 17$, in eight mice). For comparison, R_{in} for regular-spiking non-pyramidal cells was 98.8 ± 12 MΩ ($n = 5$, from five mice in the first month of life).

Probes). For VGAT and polyclonal PV: indocarbocyanine Cy5-conjugated anti-rabbit antibody, made in donkey (DAR-Cy5, 1/200; Jackson Immunoresearch Laboratories Inc., West Grove, PA). For monoclonal PV: indocarbocyanine Cy3-conjugated anti-mouse IgG, made in donkey (DAM-Cy3, 1/200; Jackson Immunoresearch Laboratories). For SOM: Alexa-568 labeled anti-rat IgG, made in donkey (DARat-Alexa 568, 1/200; Molecular Probes).

Test of nAChR antibodies

As is well known, the use of nAChR antibodies for immunocytochemistry can be problematic (Moser et al., 2007). We previously tested AB5590 (Millipore, anti-α4) in human cell lines (HEK 293) transiently transfected with several nAChR subunit combinations (Aracri et al., 2010). We thus verified that AB5590 binds to $\alpha4^*$ nAChRs, although some cross-reactivity with other nAChR subunits or membrane proteins cannot be excluded. This was the essential point in the present study, in which immunocytochemistry is applied to provide a better spatial definition of the electrophysiological results.

Analysis of colocalization

Confocal micrographs were acquired with a Leica TCS SP2 confocal microscope and Confocal Software (Leica Microsystems). Resolution (300 dpi), brightness, and contrast were optimized by using Adobe Photoshop CS2 9.0 (Adobe Systems, San Jose, CA). Non-overlapping pictures (40×) were acquired from layer V, to test immunolabeling in not less than three cortical fields per mouse, from different sections containing Fr2. For two-color analysis, sections were excited at 488, 568 and 650 nm. To avoid signal crosstalk, fluorescence of Alexa 488 (green), and Cy5 (blue) or Cy3 (red) was detected sequentially. Colocalization of α4 nAChR with VGAT, PV or SOM was determined with the same software, as previously described (Aracri et al., 2013). Merged antigen localization is indicated by white signals. Images in Fig. 6A–C result from analysis of cytofluorograms, by coupling two channel at a time (red/blue, and green/blue), to identify the three types of synaptic terminals indicated by the arrows. The overlapping area between the red (PV or SOM; the latter was changed to blue, for reader's convenience, in Fig. 7E, F) and the green signal (α4 nAChR), was determined on single-plane images. To calculate the Manders coefficients, we applied the JACoP plug-in for ImageJ software (Bolte and Cordelières, 2006). For 3D reconstruction analysis (Fig. 6D–F), z-stack series of 30 images (1024 × 1024 pixels), spaced by 333 nm, were acquired at 126× magnification, to obtain a 10-μm stack. Images were analyzed with Imaris software (Bitplane, Zurich, Switzerland). Each stack was pre-processed with a 3D gaussian filter to reduce background noise, without altering the signal distribution. Neuronal PV+ somata and terminals (red signal) were reconstructed by isosurfaces, thus obtaining information about their volume, surface, shape and position. Next, the VGAT+ synaptic terminals (blue) were identified by spheric isosurfaces. These were centered on the point giving maximal signal intensity for each terminal, and their diameter was set based on the typical synaptic dimension. The same procedure was applied for the green channel (α4 nAChR subunit). After defining the two populations, they were filtered based on their distance from the soma surface, by eliminating those falling outside of the imposed limits (500 nm). The result was further filtered by retaining only the blue structures overlapping or contiguous to a green signal (max 500 nm between the structure centers).

Statistical analysis

The distributions of IPSC amplitudes and interevent intervals were analyzed in each cell with the Kolmogorov–Smirnov (KS) test, on at least 2-min continuous recording for each experimental condition (never containing less than ~250 events). The average results of multiple experiments are given as mean values ± SEM. Unless otherwise indicated, statistical comparisons between two populations of data were carried out with paired Student's *t*-test, at the indicated level of significance (p), after testing that the data were normally distributed (with KS test), with equal variances (with *F*-test). The number of indicated experiments (n) refers to the number of tested cells or cortical fields. The number of mice is also indicated. When two experiments were carried out in two slices from the same animal, the results were averaged to avoid bias from nested data (Aarts et al., 2014).

RESULTS

The Fr2 region displays a prominent layer V, with large pyramidal neurons. In this layer, FS cells constitute the majority of PV+ neurons (Kawaguchi and Kondo, 2002; Rudy et al., 2011), and are well recognized by firing pattern and spike width (Connors and Gutnick, 1990). Puta-

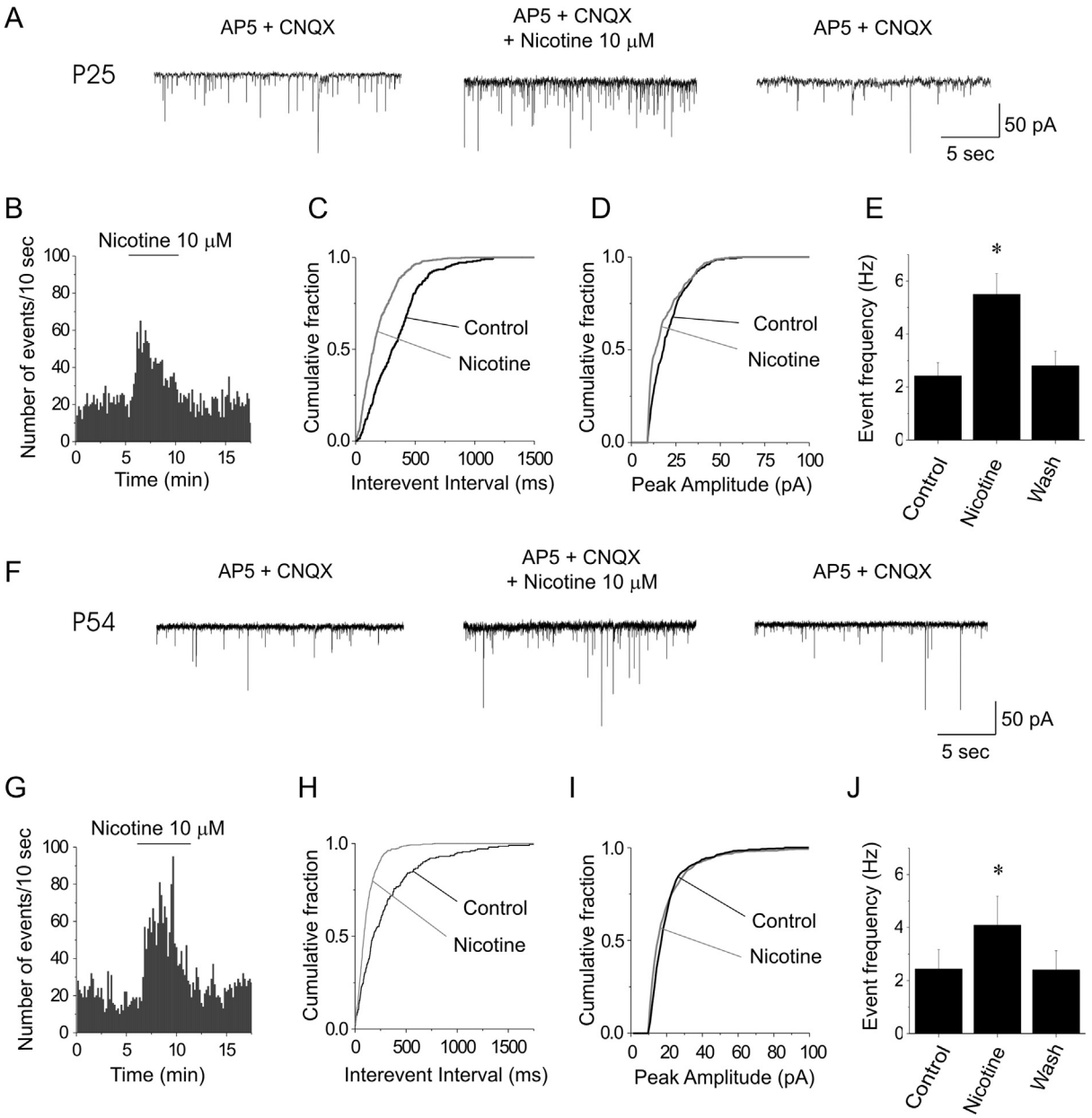

Fig. 2. Nicotine stimulates IPSCs in FS cells at different postnatal ages. (A) IPSC traces, in the presence of AP5 and CNQX, in a slice from a P25 mouse (same cell as in Fig. 1B). Nicotine reversibly increased the IPSC frequency. (B) Time course of the nicotine effect. Bars give the number of IPSCs measured within consecutive 10-s intervals, in the indicated conditions. (C) Distribution of the interevent intervals calculated for 2 min before (Control) and during nicotine application. Nicotine significantly decreased the intervals between IPSCs ($p < 0.01$; KS test). Analogous results were obtained in all the other similar experiments. (D) Amplitude distribution of the IPSCs recorded for 2 min in the indicated conditions. In all tested neurons, nicotine had no effect on the distribution of the IPSC amplitudes (KS test). (E) Average effect of nicotine on IPSC frequency in slices from mice aged P16–P32. Bars give the mean IPSC frequency, calculated as illustrated in the previous panels. Nicotine approximately doubled the IPSC frequency. (F) Same as (A), except that the slice was prepared from a P54 mouse (same cell as in Fig. 1B). (G) Time course of the nicotine effect, analyzed as in (B). (H) Distribution of the interevent intervals in this experiment, analyzed as in (C). Nicotine significantly decreased the interevent intervals ($p < 0.01$; KS test). Analogous results were obtained in the other similar experiments. (I) Amplitude distribution of the IPSCs analyzed as in (D). In 16 out of 17 neurons (from mice older than P45), nicotine had no effect on the distribution of the IPSC amplitudes (KS test). (J) On average, nicotine increased the IPSC frequency by ~60%. * statistically significant ($0.01 < p < 0.05$).

tive FS cells were first identified based on non-pyramidal morphology with relatively small round cell body (Fig. 1B). Next, the firing pattern was assessed by applying consecutive 0.5-s depolarizing currents (20-pA steps). Above threshold, FS cells displayed action potential (AP) frequencies of up to 80–100 Hz (with 200-pA stimulus), spike width ~0.7 ms (at half-maximal AP amplitude), and first AHP of approximately −14 mV, consistent with previous results in mouse neocortex (Couey et al., 2007; Okaty et al., 2009; Tai et al., 2014; Yang et al., 2014). Fig. 1C shows typical cell firing in two FS cells from, respectively, a P25 and a P54 mice. The firing frequency as a function of injected current is plotted in Fig. 1D, for a representative sample of cells ($n = 10$).

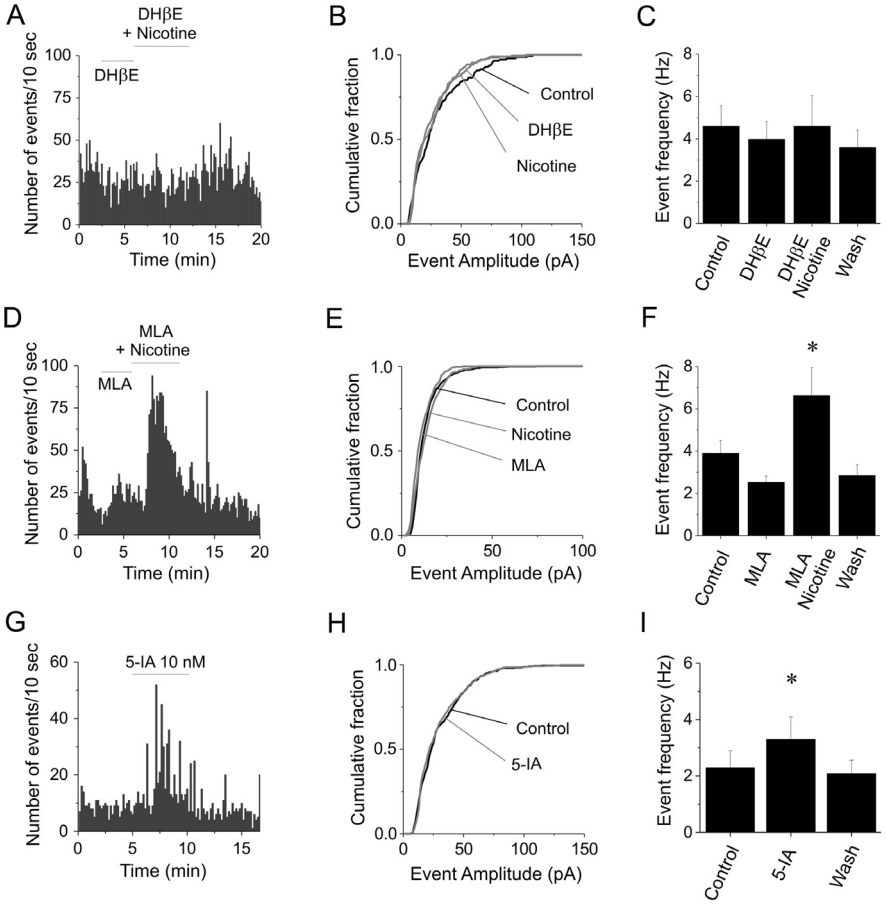

Fig. 3. The effects of DHβE, MLA and 5-IA. Data analysis was as illustrated in Fig. 2. (A) Time course of the IPSC frequency in a representative experiment. DHβE blocked the nicotine-dependent increase in IPSC frequency. (B) Corresponding distribution of the IPSC amplitudes, in the indicated conditions. Nicotine did not change the IPSC amplitude distribution, in the presence of DHβE (KS test). Similar results were obtained in nine cells. (C) On average, DHβE blocked the action of nicotine on IPSC frequency. (D) Same as (A), but in the presence of MLA, which did not block the nicotine-dependent increase in IPSC frequency. (E) Corresponding distribution of the IPSC amplitudes. In nine cells, no significant difference was observed in the distribution of IPSC amplitudes in the presence of MLA and MLA plus nicotine (KS test). (F) On average, nicotine more than doubled the IPSC frequency observed in the presence of MLA. (G) Time course of the stimulation produced by 5-IA on the IPSC frequency, on cells sampled in the first postnatal month. (H) Corresponding distribution of the IPSC amplitudes. In 6 cells, no significant effect was produced by 5-IA on the IPSC amplitude distribution (KS test). (I) On average, 5-IA increased the IPSC frequency by ~45%. * statistically significant ($0.01 < p < 0.05$).

The electrophysiological parameters of FS cells at different ages are shown in Table 1. No statistical differences were observed between the age groups. The other major population of interneurons we routinely observed was constituted by regular-spiking non-pyramidal cells (Kawaguchi, 1993; Couey et al., 2007; McGarry et al., 2010), showing AP frequencies of 30–40 Hz (with 200-pA stimulus), more pronounced adaptation compared to FS cells, spike width generally larger than 1 ms, and shallow AHP. The effect of nicotine was not tested in these cells.

Nicotine stimulated GABA release onto FS cells

Because the Nernst potential for Cl^- was −16 mV, we recorded spontaneous postsynaptic GABAergic currents as inward events at −70 mV, after blocking ionotropic glutamate receptors with 40 μM AP5 and 10 μM CNQX. These conditions were chosen to study the GABAergic events around V_{rest}. For simplicity, we refer to these currents as IPSCs, although in physiological ionic conditions they would be outward events. The persistence of GABAergic synaptic activity in the absence of glutamatergic transmission can be attributed to the pacemaker properties of several populations of neocortex cells, such as the Martinotti interneurons in layer V (Le Bon-Jego and Yuste, 2007), and possibly other populations in nearby layers, whose neurochemical nature is still uncertain (e.g., Wenger-Combremont et al., 2016).

To study the nAChR-dependent effects, nicotine was preferred to ACh, to avoid applying muscarinic antagonists, which can affect nAChRs (Zwart and Vijverberg, 1997). Nicotine was applied at 10 μM, which is close to the peak of the 'window' (i.e., steady state) current for α4β2 and α7 receptors (e.g., Fenster et al., 1997; Brusco et al., 2015), thus producing the maximal tonic effect (Aracri et al., 2010). In this way, we could test the response of both nAChR subtypes in conditions that mimic diffuse ACh transmission. Representative IPSC traces are shown in Fig. 1E, in the absence and presence of nicotine. Consistent with the GABAergic nature of IPSCs, 10 μM bicuculline inhibited all synaptic events. The effect of nicotine on IPSCs is quantified in Fig. 2. Representative IPSC traces in the absence or presence of nicotine for a P25 mouse are shown in Fig. 2A. The time course of the nicotine effect is illustrated by plotting the number of IPSCs in consecutive 10-s intervals, in the indicated conditions (Fig. 2B). Nicotine was applied after allowing the spontaneous IPSC frequency to stabilize for about 5 min. The drug augmented the spontaneous IPSC frequency, as shown by the cumulative distribution of the interevent intervals (Fig. 2C), without significantly altering the distribution of amplitudes (Fig. 2D). In nine similar experiments on slices prepared from seven mice (between the 3rd and the 5th postnatal week), nicotine brought the IPSC frequency from 2.42 ± 0.5 Hz to 5.5 ± 0.78 Hz ($0.01 < p < 0.05$; DF = 6). After washout, the IPSC frequency was 2.8 ± 0.56 Hz (Fig. 2E). No effects were observed on the corresponding IPSC kinetics. The IPSC activation was measured as the 10% to 90% rise-time. This latter, in the absence and presence of nicotine

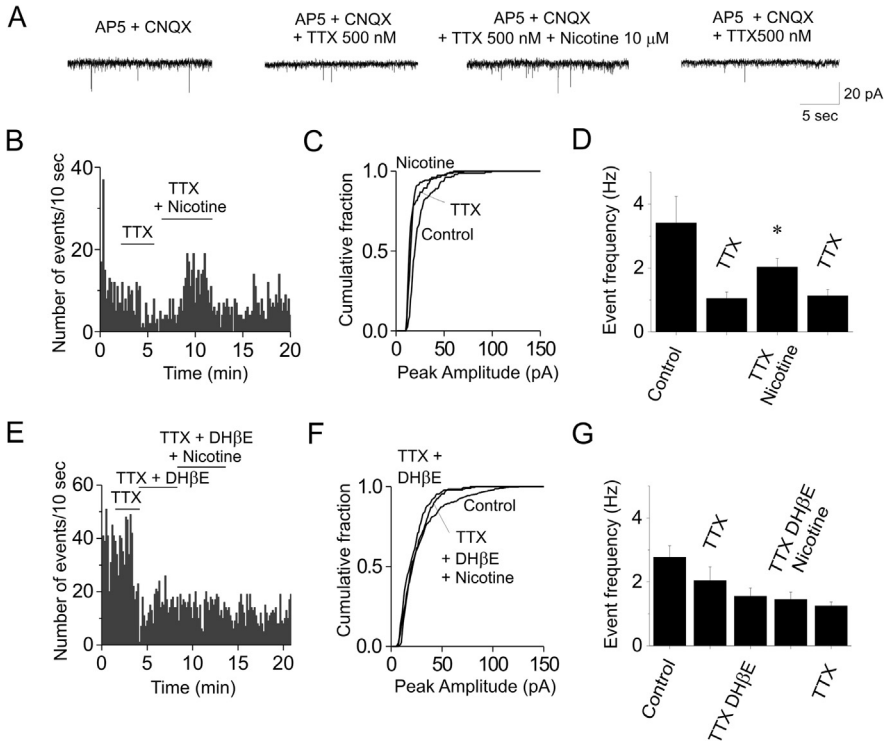

Fig. 4. Heteromeric nAChRs stimulate the mIPSC's. Data analysis was as in Fig. 2. (A) Representative IPSCs in the indicated conditions. After TTX had revealed the mIPSCs, nicotine increased their frequency, in a reversible way. (B) Time course of the IPSC frequency in the same experiment. (C) Corresponding IPSC amplitude distribution, in the indicated conditions. TTX decreased the IPSC amplitudes. No further effect was produced by nicotine in nine neurons (KS test). (D) On average, nicotine approximately doubled the mIPSC frequency. (E) Representative time course of the effect of nicotine plus DHβE. The latter blocked the IPSC stimulation produced by nicotine. (F) Corresponding IPSC amplitude distribution. TTX revealed miniature events. No further effect was produced by either DHβE or DHβE plus nicotine (KS test). The same was observed in nine similar experiments. (G) On average, nicotine had no effect on mIPSCs, in the presence of DHβE.

was, respectively, 0.75 ± 0.04 ms and 0.68 ± 0.06 ms (NS; DF = 6). The corresponding time constants of the IPSC current decay were 8.6 ± 1.28 ms and 8.7 ± 1.13 ms (NS; DF = 6).

In mouse development, conspicuous variations in nAChR subunit expression occur before P21, which subside during the second month of postnatal life (Molas and Dierssen, 2014). Hence, we repeated the above experiments in older mice (P45–P63). In these, the nicotinic effect on IPSCs was similar to the one observed at younger stages, although the stimulation was less marked. A representative experiment is illustrated in Fig. 2F–I. On average (n = 12, from 8 mice), nicotine augmented the spontaneous IPSC frequency from 2.44 ± 0.73 Hz to 4.09 ± 1.1 Hz ($0.01 < p < 0.05$; DF = 7). After washout, the IPSC frequency was 2.4 ± 0.55 Hz (Fig. 2J). Once again, no effect was observed on IPSC amplitudes and kinetics. The IPSC rise-times in the absence and presence of nicotine were, respectively, 0.62 ± 0.04 ms and 0.63 ± 0.02 ms (NS; DF = 7). The corresponding time constants of the IPSC current decay were 6.3 ± 0.26 ms and 5.5 ± 0.16 ms (NS; DF = 7).

The effect of nicotine depended on α4* nAChRs

The role of α4* and α7* nAChRs can be discriminated by blocking these receptors, respectively, with 1 μM DHβE and 10 nM MLA (Harvey et al., 1996; Murray et al., 2012). After treating the cells with one of the blockers for 3–4 min, 10 μM nicotine was added. Data analysis was carried out as in Fig. 2. DHβE abolished the stimulatory effect of nicotine on the IPSC frequency. A representative example is illustrated in Fig. 3A. In the same cell, no effect was observed in the IPSC amplitudes (Fig. 3B). The effects observed in a series of similar experiments carried out on slices from young mice (3rd to 5th postnatal week) are given in Fig. 3C. On average (n = 9, from seven mice), IPSC frequencies were 4.6 ± 0.97 Hz (control), 3.98 ± 0.85 Hz (DHβE), 4.6 ± 1.44 Hz (nicotine + DHβE; NS compared to DHβE; DF = 6), and 3.6 ± 0.81 Hz after washout. Analogous results were obtained in mice aged P45–P60 (n = 6; not shown). In contrast, MLA produced no alteration of the effect of nicotine (Fig. 3D). On average (n = 9, in nine mice), the IPSC frequency was 3.89 ± 0.6 Hz (control), 2.53 ± 0.86 Hz (MLA), 6.63 ± 1.32 Hz (MLA + nicotine; $p < 0.01$ compared to MLA; DF = 8), and 2.86 ± 0.5 Hz after washout (Fig. 3F). Once again, the IPSC amplitudes were not altered (Fig. 3E), consistent with the effect produced by nicotine alone. We conclude that the tonic stimulation produced by nicotine on the IPSCs recorded on FS interneurons was largely mediated by α4* nAChRs.

5-IA stimulated IPSCs in FS cells

To better define the nAChR subtype involved in IPSC regulation, we applied a submaximal concentration of 5-IA (10 nM), which specifically activates β2* receptors (Mogg et al., 2004). The effect of 5-IA in a representative experiment is shown in Fig. 3G. The drug increased the IPSC frequency, but not the amplitude (Fig. 3H). On average (n = 6, from six mice in the 4th postnatal week; Fig. 3I), 5-IA brought the IPSC frequency from 2.28 ± 0.61 Hz (Control), to 3.3 ± 0.8 Hz (5-IA; $0.01 < p < 0.05$; DF = 5). After recovery, the IPSC frequency was 2.08 ± 0.47. Considering that 10 nM 5-IA is known to activate about 40% of the maximal nicotinic current (Mogg et al., 2004), our data are consistent with those obtained with nicotine. Overall, the results obtained with DHβE, MLA and 5-IA suggest that GABA release

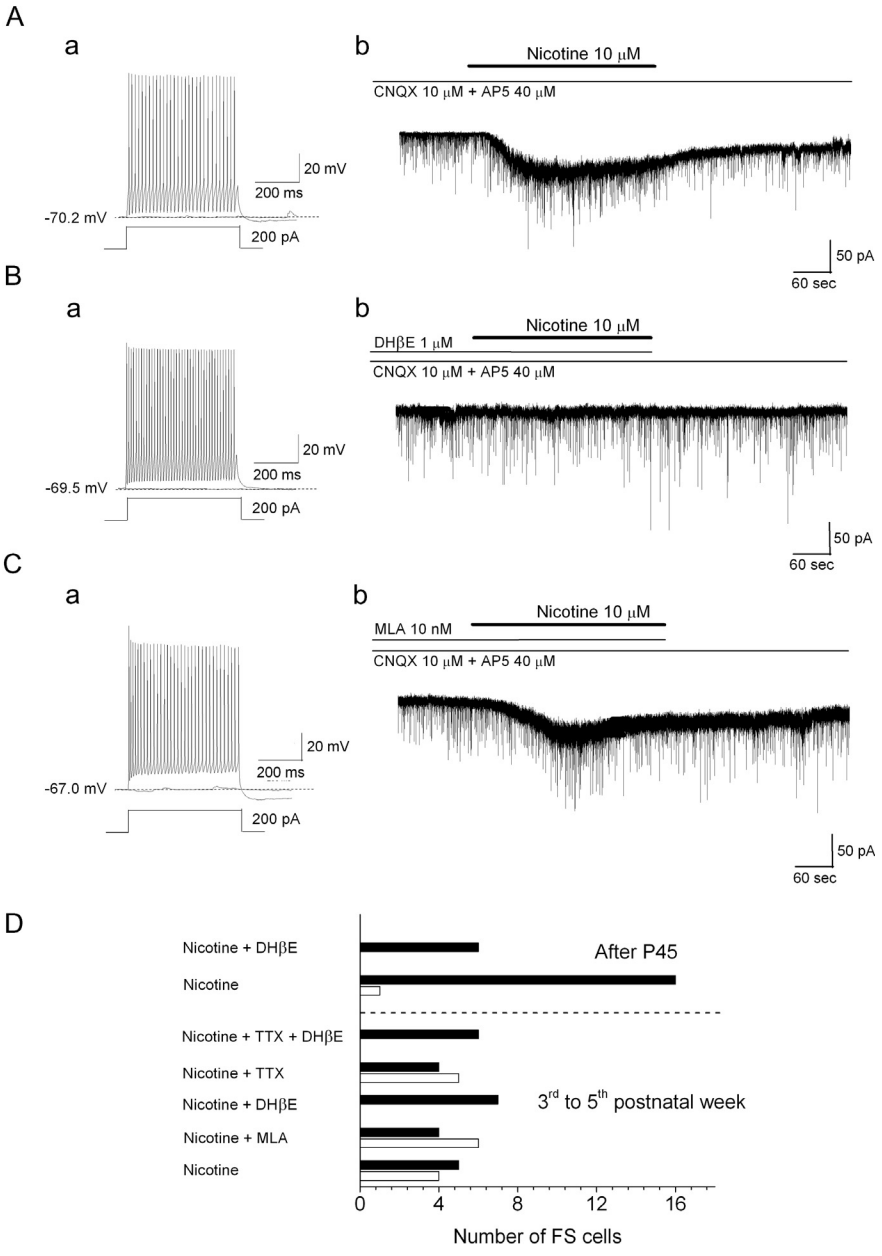

Fig. 5. Heteromeric nAChR currents in FS cells. (A) Representative experiment on a FS cell. The firing pattern in response to a 200-pA injection is shown in (a). After testing cell firing, the neuron was voltage-clamped at −70 mV, and nicotine was added (b). (B) Same as (A), except that the FS cell was treated with nicotine plus DHβE (b). (C) Same as (A), except that the FS cell was treated with nicotine plus MLA (b). (D) In a fraction of the tested cells, nicotine elicited an inward slowly desensitizing current, which was also observed when nicotine was applied in the presence of MLA, but never in the presence of DHβE. Bars represent the number of FS cells displaying (white) or not (black) whole-cell currents activated by nicotine. The results for cells from younger mice (First month) are given for the indicated treatments. For cells sampled after P45, the results are relative to treatment with nicotine or nicotine + DHβE (as indicated). The results obtained in the two age groups are separated by the dashed horizontal line.

onto FS cells was mainly regulated by $\alpha4\beta2^*$ nAChRs, in conditions of tonic agonist application.

Heteromeric nAChRs regulate mIPSCs in FS cells

The spontaneous IPSCs are constituted by a mixture of AP-dependent larger release events, and AP-independent mIPSCs (e.g., in the context of nicotinic regulation, Lambe et al., 2003; Klaassen et al., 2006; Aracri et al., 2010). Hence, the effect of nicotine on spontaneous IPSCs could depend on direct stimulation of presynaptic terminals, or on increase in AP-dependent release events, caused by activation of somatic currents on presynaptic GABAergic cells, or both. The direct effect of nicotine on synaptic terminals can be revealed by studying the effect on mIPSCs, which are isolated by blocking cell firing with 0.5 μM TTX. Representative current traces are shown in Fig. 4A, along with the corresponding IPSC time course (Fig. 4B), and amplitude distribution (Fig. 4C), in the indicated conditions. After TTX had revealed the mIPSCs, 10 μM nicotine was added. On average (n = 10, from seven mice in the 3rd to 5th postnatal week; Fig. 4D), nicotine brought the mIPSC frequency from 1.05 ± 0.2 Hz (TTX) to 2.03 ± 0.27 Hz (nicotine + TTX; $0.01 < p < 0.05$; DF = 6). After recovery, mIPSC frequency was 1.13 ± 0.20 Hz (in TTX, after washout of nicotine). Negligible effects were produced by nicotine on the mIPSC kinetics. The IPSC risetimes were 0.57 ± 0.04 ms (TTX) and 0.57 ± 0.05 ms (TTX + nicotine; NS; DF = 9). The corresponding time constants of IPSC current decay were 8.93 ± 1.28 ms, and 10.1 ± 1.5 (NS; DF = 9).

Moreover, after TTX had produced the expected reduction in IPSC frequency (Fig. 4E) and amplitude (Fig. 4F), subsequent application of 1 μM DHβE, and DHβE plus nicotine, produced no further effect. The results obtained on mIPSCs in the presence of DHβE are summarized in Fig. 4G. On average (n = 6, from five mice), nicotine brought the mIPSC frequency from 1.55 ± 0.26 Hz (TTX + DHβE) to 1.45 ± 0.23 Hz (TTX + DHβE + nicotine; NS; DF = 4). After recovery, the mIPSC frequency was 1.25 ± 0.12 Hz (in TTX). These results are consistent with the hypothesis that $\alpha4\beta2^*$ receptors regulate GABA release from presynaptic terminals adjacent to FS cells, in Fr2 layer V.

Whole-cell nicotinic currents on FS cells

In the Fr2 slices prepared from young mice (3rd to 5th postnatal week), nicotine also activated typical slowly

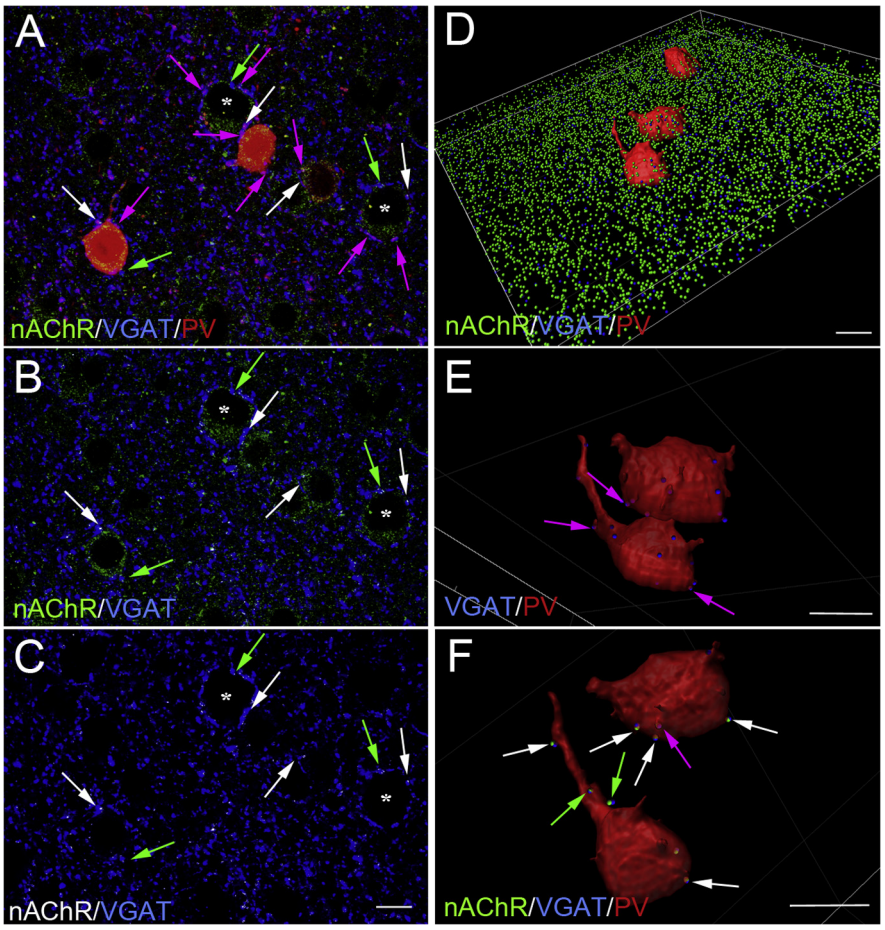

Fig. 6. Localization of nAChRs on GABAergic terminals, in Fr2 layer V, at different postnatal ages. (A) Triple labeling of α4 nAChR (green), VGAT (blue) and PV (red), at P60. Few GABAergic PV+ terminals (purple arrows), contact PV+ cell bodies, and are more frequently found around PV− somata (asterisks), which are likely pyramidal cells. α4 nAChRs are expressed on a few VGAT+ GABAergic terminals (green arrows), some of them being also PV+ (white arrows). Colocalization of α4 and VGAT is indicated by the white puncta. (B) Detail of (A), but highlighting the α4 nAChR and VGAT signals. (C) Same as (B), after deletion of the global α4 nAChR labeling. (D) 3D reconstructed image of three PV+ neurons, in a section with triple labeling of α4 nAChR (green), VGAT (blue) and PV (red), at P40. (E) Two neurons are magnified, showing VGAT+/PV+ terminals (purple arrows) contacting PV+ cell bodies. (F) Same field as in (E), but further magnified, rotated, and displaying also the α4 nAChR signal (green). Green arrows point to α4+/VGAT+ synaptic boutons and white arrows point to α4/VGAT/PV+ terminals, both contacting PV+ cell bodies. Scale bars = 10 μm. (For interpretation of the references to colour in this figure legend, the reader is referred to the web version of this article.)

desensitizing inward currents, in a fraction of the tested FS cells, at −70 mV. A representative example is given in Fig. 5A. Whole-cell currents elicited by nicotine were also found in a fraction of the cells pre-treated with MLA (an example is shown in Fig. 5C), but never in the presence of 1 μM DHβE (Fig. 5B). Overall, 10 out of 19 FS cells displayed whole-cell currents elicited by nicotine, irrespectively of whether MLA was present or not (Fig. 5D). The observed frequencies for this group of mice are consistent with the hypothesis that the observed nicotinic currents depended on DHβE-sensitive and MLA-insensitive heteromeric nAChRs ($p < 0.05$ with Fisher's exact test; comparison between Nicotine + DHβE and Nicotine + MLA). Similar results were obtained in the presence of TTX, with 5 out of 9 cells displaying somatic nAChRs, as compared to 0 out of 6 cells treated by TTX + DHβE (Fig. 5D). However, in older mice (P45-P63), only 1 out of 17 FS cells displayed measurable somatic nAChR currents, as compared to 0 out of 6 cells in the presence of DHβE (Fig. 5D). We conclude that, in the first weeks of postnatal life, layer V FS cells can also express functional α4β2* nAChRs on the somatic compartment, in Fr2. This suggests that both somatic and presynaptic components may contribute to the tonic stimulation exerted by heteromeric nAChRs on the IPSCs recorded in FS cells. However, the contribution of the somatic currents considerably decreased with mice age.

The somatic effect of nicotinic agonists on FS cells was further characterized at physiological Cl^- concentration (to avoid interference by $GABA_A$ currents). Application of 10 nM 5-IA brought the cells' V_{rest} from −67 ± 0.49 mV to −63 ± 0.86 mV ($0.01 < p < 0.05$; $n = 5$, from four mice in the first postnatal month; DF = 3), with small effects on AP threshold (from −40 ± 1.7 mV to −38 ± 1.7 mV), rheobase (from 90 ± 10 pA to 80 ± 9 pA), and input resistance (R_{in}, from 69 ± 8 MΩ to 71 ± 9.5 MΩ). We conclude that, in a fraction of FS neurons, direct cell depolarization can be produced by activating heteromeric α4β2* nAChRs.

Localizing α4* nAChRs on GABAergic terminals adjacent to GABAergic cells

We sought independent evidence that α4 nAChR subunits are expressed in GABAergic terminals forming synapses with FS neurons. Hence, we immunocytochemically labeled α4 nAChR, PV (to mark putative FS cells), and VGAT (to label GABAergic terminals; Fig. 6A). First, we analyzed double labeling of α4 and VGAT (Fig. 6B). Overlap of the two signals (white dots) was indicated by qualitative colocalization analysis (Fig. 6B). To allow better appreciation of our signals, these colocalization puncta were also displayed in Fig. 6C, in which the global α4 nAChR labeling was removed. These results suggest that α4* nAChR is localized in a fraction of the GABAergic terminals.

Next, we studied whether a fraction of α4+/VGAT+ terminals also expressed PV and was adjacent to PV+ cell bodies (putative FS cells). This was obtained by analyzing the separate 2D cytofluorograms (not shown) for PV/VGAT and α4/VGAT related to Fig. 6A, where

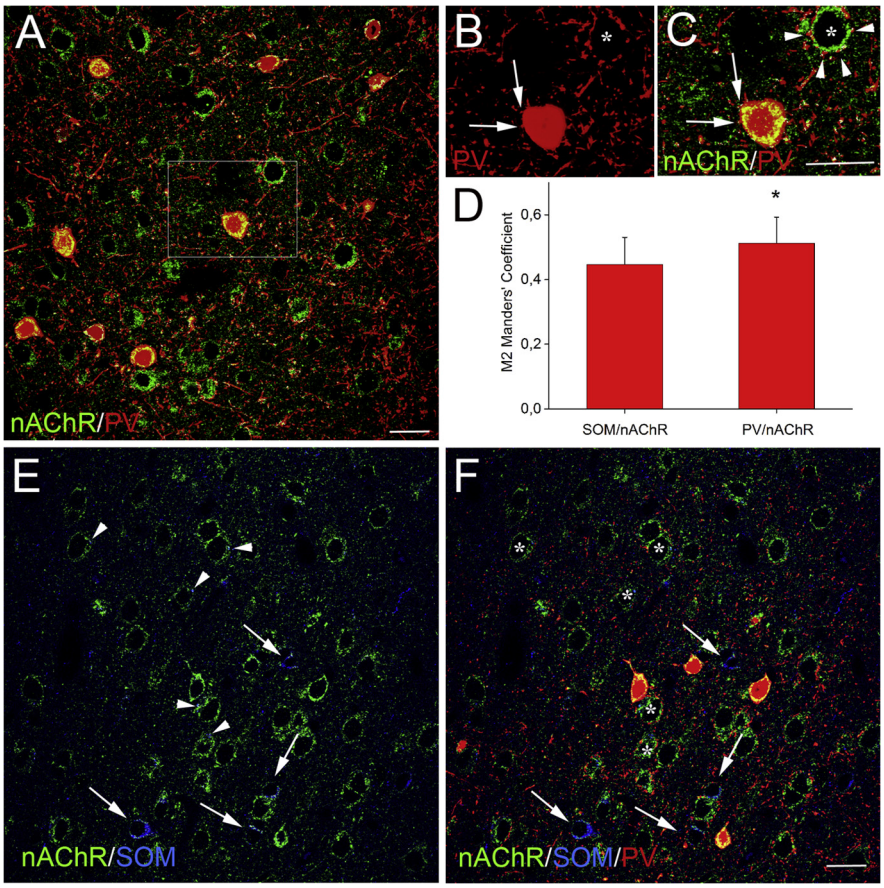

Fig. 7. Colocalization of α4 nAChR, PV and SOM, in Fr2 layer V, at P90. (A) Double labeling of α4 nAChR (green) and PV (red). Colocalization is indicated by the white spots. (B) Magnification of the boxed area in (A). Only PV labeling is shown. Asterisk marks a PV− neuron. (C) Same as (B), but showing both nAChR (green) and PV (red) signal. Colocalization analysis showed two white spots (arrows) on a PV+ cell body (corresponding to the PV+ puncta indicated by the arrows in (B)). A larger number of colocalization spots (arrowheads) were observed on the PV− neuron. (D) M2 Manders' coefficients, indicating the fraction of SOM or PV signal that is also positive for α4 nAChR. Significantly higher colocalization was observed between PV and nAChR than between SOM and nAChR. (E) Double labeling of α4 nAChR (green), and SOM (blue). The α4/SOM colocalization (white signal) was concentrated in SOM+ neurons (arrows) and only in rare puncta (arrowheads) contacting PV− neurons. (F) Same field as in (E), but also showing the PV signal (red). Asterisks mark the PV− neurons. Scale bars = 20 μm. (For interpretation of the references to colour in this figure legend, the reader is referred to the web version of this article.)

white arrows point to α4/PV/VGAT colocalization spots, i.e. GABAergic PV+ terminals contacting PV+ cell bodies, and expressing nAChR (Fig. 6A–C). Other VGAT+ synaptic terminals juxtaposed with PV+ interneurons display either only α4 nAChR (green arrows in Fig. 6A–C) or only PV (purple arrows in Fig. 6A). All three types of synaptic terminal were also found adjacent to large PV− neurons (putative pyramidal cells; Fig. 6A–C). To further define the synaptic structures in our triple VGAT/PV/α4 immunolabeled sections, we performed a 3D reconstruction from 10-μm stacks of confocal images. This allowed to better examine the interactions between PV+ neurons and the few GABAergic (VGAT+) synaptic terminals expressing PV and/or α4 nAChR subunit (Fig. 6D). Consistent with 2D images, a few PV+/VGAT+ terminals were found to contact other PV+ cells (Fig. 6E). Some of these terminals also expressed α4 nAChR (Fig. 6F). These results point to the presence of synaptic interaction between PV+ neurons expressing α4* nAChRs.

Comparison of α4* nAChR expression in PV+ and SOM+ interneurons

We first examined the α4/PV colocalization at P90 (Fig. 7A). In agreement with the results obtained at earlier stages, some PV+/α4+ cell bodies were juxtaposed with few PV+ puncta (Fig. 7B) that also expressed α4 (Fig. 7C). Next, we labeled SOM to mainly mark the Martinotti interneurons. These largely account for the regular-spiking non-pyramidal cells (Kawaguchi and Kondo, 2002; McGarry et al., 2010), i.e. the other major interneuron population we observed in layer V by electrophysiological methods. Differently from what was observed with PV+ cells, the α4/SOM colocalization was concentrated in SOM+ cell bodies (Fig. 7E), clearly distinct from the PV+ somata (Fig. 7F). Rare puncta showing α4/SOM colocalization (Fig. 7E) were adjacent neither to SOM+, nor PV+ neuronal bodies (Fig. 7E, F). This is consistent with the tendency of SOM+ terminals to form synapses on non-somatic cell compartments (Harris and Mrsic-Flogel, 2013; Kepecs and Fishell, 2014). These results suggest that SOM+ interneurons are mainly regulated by α4* nAChRs at the somatic, i.e. non-synaptic, level. Finally, the quantitative analysis of total (i.e. neuronal cell bodies, processes and puncta) colocalization between either SOM and α4, or PV and α4, showed that the amount of PV+/α4+ structures was significantly higher than the amount of the SOM+/α4+ ones (Fig. 7D). The M2 Manders coefficients (in layer V of Fr2 cortical fields) were 0.446 ± 0.08 for SOM and 0.512 ± 0.08 for PV ($p = 0.003$; $n = 11$ images from three different mice; DF = 2).

Taken together, our immunocytochemical results suggest that both PV+ and SOM+ cells can be modulated by α4* nAChRs. In agreement with patch-clamp results on FS cells, in PV+ cells regulation at the synaptic level tends to prevail, starting from the second postnatal month.

DISCUSSION

Here, we have shown that tonic activation of heteromeric nAChRs regulates the IPSCs recorded on FS cells, in layer V of the mouse Fr2 area. Our pharmacological results indicate that the IPSC stimulation mainly

depends on activation of $\alpha4\beta2^*$ receptors. MLA is a competitive antagonist of $\alpha7$ receptors, with IC_{50} in the pM range (Palma et al., 1996), whereas micromolar concentrations are necessary to block $\alpha4\beta2$ (Drasdo et al., 1992; Buisson et al., 1996). DHβE is a competitive antagonist of $\alpha4^*$ nAChRs, with IC_{50} of ~80 nM for $\alpha4\beta2$ (Buisson et al., 1996), and reported IC_{50} values between 2 and 20 μM for $\alpha7$ receptors (Bertrand et al., 1992; Chavez-Noriega et al., 1997). Therefore, inhibition by DHβE, but not MLA, is a good evidence of implication of $\alpha4^*$ nAChRs. Moreover, 5-IA was used at a concentration specific for $\beta2^*$ receptors (Mogg et al., 2004), and particularly the high-affinity $(\alpha4)2(\beta2)3$ stoichiometry (Zwart et al., 2006). Although other nAChR subtypes can be targeted by 5-IA (such as $\alpha6\beta2^*$), in murine PFC the expression of $\alpha4\beta2^*$ is largely prevalent (Zoli et al., 2015).

In the hippocampus, heteromeric nAChRs are expressed in several interneuron types, including the PV + (e.g., Ji and Dani, 2000; Griguoli and Cherubini, 2012). In contrast, a comprehensive picture of nAChR expression and function in the neocortex is not available. In rat, nAChRs are not detectable in FS cells in visual (Xiang et al., 1998) and motor (Porter et al., 1999) cortex, but they are widely expressed in layer I interneurons, which regulate inhibition of interneurons in layers II/III (Christophe et al., 2002). Expression of $\alpha4^*$ nAChRs was also observed in layer IV GABAergic neurons of somatosensory areas, but the specific cell-type distribution is unclear (Brown et al., 2012). In deep layers of medial PFC of mice (Couey et al., 2007) and rats (Gulledge et al., 2007), $\alpha4^*$ nAChR expression is mainly restricted to non-FS cells. Our results with SOM labeling confirm in more dorsal PFC regions that $\alpha4\beta2^*$ receptors are found in non-FS cells. However, in Fr2 we also observed that a significant fraction of FS cells express whole-cell currents carried by heteromeric nAChRs, in the first postnatal month (Fig. 5).

Although still fragmentary, the above evidences suggest that differences in the pattern of cholinergic stimulation exist among different PFC regions. This notion would agree with the morphological observation that the cholinergic fibers innervating the PFC are scarcely collateralized, further indicating that there may be area-specific mechanisms of cholinergic regulation of neocortical circuits (Price and Stern, 1983; Walker et al., 1985; Koliatsos et al., 1988; Sarter et al., 2009). The complexity of such regulatory pattern may be related to a higher degree of functional flexibility in the regions directly implicated in elaborating the decision-execution prefrontal tasks. These areas could be physiologically more similar to the Primate neocortex, where nicotinic targeting of FS cells seems more common (Disney et al., 2007, 2012; and references therein).

Nicotinic regulation of GABAergic synaptic terminals and cell bodies

Our results on mIPSCs as well as immunocytochemistry point to a direct nicotinic stimulation of GABAergic terminals. The neuronal nAChRs are generally permeable to cations, with poor selectivity between Na^+ and K^+ (Nutter and Adams, 1995). Hence, once activated around V_{rest}, they produce cell depolarization, with ensuing excitatory effects. The nAChR permeability to calcium (P_{Ca}) depends on channel subtype. Heteromeric receptors present a P_{Ca}/P_{Na} ratio of ~2 (Fucile, 2004). Hence, we attribute our results to a combination of voltage-dependent activation of presynaptic calcium channels and direct stimulation of exocytosis by Ca^{2+} influx through nAChRs. That the latter can contribute to neurotransmitter release is confirmed by previous studies showing that a DHβE-sensitive effect of nicotine on GABA release is revealed when mIPSCs are registered in presence of both TTX and Cd^{2+} (Klaassen et al., 2006; Aracri et al., 2010). At concentrations lower than 100 μM, Cd^{2+} reversibly blocks long-lasting voltage-gated calcium channels (Fox et al., 1987). Therefore, in analogy with what was described for $\alpha7$ receptors, heteromeric nAChRs may be able to stimulate neurotransmitter release by a Ca^{2+}-dependent and SNARE complex-dependent exocytosis (Albuquerque et al., 2009).

As to the possible postsynaptic effects of nicotine, a direct modulation of $GABA_A$ receptors seems unlikely, in our conditions, as nicotine produced negligible effects on the amplitude and kinetics of both spontaneous and miniature IPSCs. However, during the first postnatal month, a significant fraction of FS interneurons expressed somatic heteromeric nAChRs. Therefore, at this stage, nAChR activation can also depolarize FS cell bodies. On a short time scale, such excitation would increase FS cell firing. The ensuing stimulation of GABA release would sum its effect to the one exerted on GABAergic terminals. The possible effects on local excitability are discussed in the next paragraph. On a medium time scale (minutes), we can speculate that the nAChR-dependent calcium entry could affect several protein kinase pathways that are known to modulate the activity of heteromeric nAChR themselves (e.g., Fenster et al., 1999). On a longer time scale, these calcium-dependent signals regulate transcription factors such as CREB (e.g., Chang and Berg, 2001; Walters et al., 2005), which could modulate the activity of both pre- and postsynaptic cells. Such effects were not observable within the time scale of our experiments, as is confirmed by the fact that the amplitude and kinetics of IPSCs were not altered by nicotine application. However, they merit further study in experimental conditions that permit long-term sampling of the postsynaptic effects.

Implications for excitability in the developing and mature PFC

The decrease in nAChR current expression we observed in Fr2 FS cells after P45 suggests that somatic nicotinic currents may be implicated in prefrontal circuit maturation. In the hippocampus, heteromeric nAChRs modulate specific GABAergic cell populations since the early postnatal stages, thus contributing to the maturation of synaptic efficacy (reviewed in Griguoli and Cherubini, 2012). Although evidence is less extensive, the GABAergic system is also thought to have developmental roles in neocortex maturation and refinement of synaptic circuits (Le Magueresse and Monyer, 2013). Therefore, our observations suggest that the direct nico-

tinic regulation of Fr2 FS cells is implicated in early stages of activity-dependent local circuit stabilization, perhaps mediated by the above-mentioned signaling mechanisms.

We cannot presently distinguish which proportion of the IPSCs we measure on FS cells depends on GABA release from other FS cells or non-FS cells. Nonetheless, our results suggest that $\alpha4\beta2^*$ nAChRs can produce network disinhibition by increasing GABA release onto interneurons in Fr2 layer V. In deep layers, nAChR stimulation is thought to produce overall excitatory effects (e.g., Poorthuis et al., 2013). Layer V, in particular, provides a major output to subcortical targets and is particularly susceptible to develop and spread hyperexcitability (Shu et al., 2003; Ozeki et al., 2009; Cammarota et al., 2013). This agrees with the well-known stimulatory effect produced by $\beta2^*$ nAChRs on glutamate release throughout the mouse PFC (Lambe et al., 2003; Couey et al., 2007; Aracri et al., 2013). However, to better define the nAChR roles on the dynamics of neocortical output as well as the possible pathological implications, it is essential to understand how nAChRs regulate the balance of excitation and inhibition in the different regions. In both hippocampus and neocortex, because of the strong local inhibitory restraint on pyramidal neurons, it is generally difficult to generate hyperexcitability in the absence of some degree of circuit disinhibition (Isaacson and Scanziani, 2011; Paz and Huguenard, 2015). These experimental observations are supported by theoretical work on recurrent network models containing balanced excitatory and inhibitory elements, showing that the network output is very sensitive to the regulation of inhibition, and that engagement of inhibitory neurons can lead to counterintuitive effects on excitability (Tsodyks et al., 1997; Murphy and Miller, 2009; Ozeki et al., 2009; Murray et al., 2014). Most experimental studies have addressed the sensory cortices, in which the relevance of circuit disinhibition for sensory elaboration and learning has been recently revealed (Letzkus et al., 2011; Pfeffer et al., 2013; Pi et al., 2013). However, the mechanisms by which the ascending regulatory systems modulate these processes are largely unknown. In layer II/III of murine sensory cortex, FS cell disinhibition was found to be indirectly regulated by non-$\alpha7$ nAChRs, which stimulate non-FS cells that form synapses onto FS neurons (Arroyo et al., 2012). Virtually nothing is known about these mechanisms in associative cortices. Our results suggest that, in Fr2, the excitatory effect previously found to depend on nAChR-mediated stimulation of glutamate release (Aracri et al., 2013) is accompanied and potentially reinforced by direct regulation of network disinhibition. Because in this region nAChRs also regulate GABA release onto pyramidal cells (Aracri et al., 2010), a full understanding of the nicotinic effects on the local balance of excitation and inhibition requires more detailed notions about the microstructure of the prefrontal circuit. From a pathophysiological standpoint, the mechanism identified in the present paper could contribute to elicit abnormal excitability in prefrontal cortices expressing hyperfunctional mutant $\alpha4\beta2$ nAChRs, such as those expressed in ADNFLE and other strictly related genetic epilepsies (Becchetti et al., 2015).

Acknowledgments—The work was supported by Telethon Italy (grant GGP12147 to AB) and by the University of Milano-Bicocca (FAR). The funding sources had no involvement in study design; in the collection, analysis and interpretation of data; in the writing of the report; and in the decision to submit the article for publication. We thank Dr. Maurizio Abbate for invaluable help in the 3D analysis of Fig. 6, and Dr. Debora Modena for carrying out some of the immunocytochemical tests. PA, SM, and AC carried out the patch-clamp experiments. PA, AC and AA performed immunocytochemistry. All the authors contributed to design the experiments and analyze the data. AB wrote the paper.

REFERENCES

Aarts E, Verhage M, Veenvliet JV, Dolan CV, van der Sluis S (2014) A solution to dependency: using multilevel analysis to accommodate nested data. Nat Neurosci 17:491–495.

Albuquerque EX, Pereira EFR, Alkondon M, Rogers SW (2009) Mammalian nicotinic acetylcholine receptors: from structure to function. Physiol Rev 89:73–120.

Alkondon M, Pereira EF, Eisenberg HM, Albuquerque EX (2000) Nicotinic receptor activation in human cerebral cortical interneurons: a mechanism for inhibition and disinhibition of neuronal networks. J Neurosci 20:66–75.

Aracri P, Consonni S, Morini R, Perrella M, Rodighiero S, Amadeo A, Becchetti A (2010) Tonic modulation of GABA release by nicotinic acetylcholine receptors, in layer V of the murine prefrontal cortex. Cereb Cortex 20:1539–1555.

Aracri P, Amadeo A, Pasini ME, Fascio U, Becchetti A (2013) Regulation of glutamate release by heteromeric nicotinic receptors in layer V of the secondary motor region (Fr2) in the dorsomedial shoulder of prefrontal cortex in mouse. Synapse 67:338–357.

Arroyo S, Bennett C, Aziz D, Brown SP, Hestrin S (2012) Prolonged disynaptic inhibition in the cortex mediated by slow, non-$\alpha7$ nicotinic excitation of a specific subset of cortical interneurons. J Neurosci 32:3859–3864.

Bacci A, Huguenard JR, Prince DA (2003) Functional autaptic neurotransmission in fast spiking interneurons: a novel form of feedback inhibition in the neocortex. J Neurosci 23:859–866.

Becchetti A, Aracri P, Meneghini S, Brusco S, Amadeo A (2015) The role of nicotinic acetylcholine receptors in autosomal dominant nocturnal frontal lobe epilepsy. Front Physiol 6:22.

Berendse HW, Galis-de Graaf Y, Groenewegen HJ (1992) Topographical organization and relationship with ventral striatal compartments of prefrontal corticostriatal projections in the rat. J Comp Neurol 316:314–347.

Bertrand D, Bertrand S, Ballivet M (1992) Pharmacological properties of the homomeric $\alpha7$ receptor. Neurosci Lett 146:87–90.

Bloem B, Poorthuis RB, Mansvelder HD (2014) Cholinergic modulation of the medial prefrontal cortex: the role of nicotinic receptors in attention and regulation of neuronal activity. Front Neural Circuits 8:17.

Bolte S, Cordelières FP (2006) A guided tour into subcellular colocalization analysis in light microscopy. J Microsc 224:213–232.

Bon-Jego Le, Yuste R (2007) Persistently active, pacemaker-like neurons in neocortex. Front Neurosci 1:1.

Brown CE, Sweetnam D, Beange M, Nahirney PC, Nashmi R (2012) $A4^*$ Nicotinic acetylcholine receptors modulate experience-based cortical depression in the adult mouse somatosensory cortex. J Neurosci 32:1207–1219.

Brusco S, Ambrosi P, Meneghini S, Becchetti A (2015) Agonist and antagonist effects of tobacco-related nitrosamines on human $\alpha4\beta2$ nicotinic acetylcholine receptors. Front Pharmacol 6:201.

Buisson B, Gopalakrishnan M, Arneric SP, Sullivan JP, Bertrand D (1996) Human $\alpha4\beta2$ neuronal nicotinic acetylcholine receptor in HEK 293 cells: a patch-clamp study. J Neurosci 16:7880–7891.

Cammarota M, Losi G, Chiavegato A, Zonta M, Carmignoto G (2013) Fast spiking interneuron control of seizure propagation in a cortical slice model of focal epilepsy. J Physiol (Lond) 591:807–822.

Cardin JA, Carlen M, Meletis K, Knoblich U, Zhang F, Deisseroth K, Tsai LH, Moore CI (2009) Driving fast-spiking cells induces gamma rhythm and controls sensory responses. Nature 459:663–667.

Chang KT, Berg DK (2001) Voltage-gated channels block nicotinic regulation of CREB phosphorylation and gene expression in neurons. Neuron 32:855–865.

Chavez-Noriega LE, Crona JH, Washburn MS, Urrutia A, Elliott KJ, Johnson EC (1997) Pharmacological characterization of recombinant human neuronal nicotinic acetylcholine receptors hα2β2, hα2β4, hα3β2, hα3β4, hα4β2, hα4β4 and hα7 expressed in *Xenopus* oocytes. J Pharmacol Exp Ther 280:346–356.

Christophe E, Roebuck A, Staiger JF, Lavery DJ, Charpak S, Audinat E (2002) Two types of nicotinic receptors mediate an excitation of neocortical layer I interneurons. J Neurophysiol 88:1318–1327.

Condé F, Maire-Lepoivre E, Audinat E, Crepel F (1995) Afferent connections of the medial frontal cortex of the rat. II Cortical and subcortical afferents. J Comp Neurol 352:567–593.

Connors BW, Gutnick MJ (1990) Intrinsic firing patterns of diverse neocortical neurons. Trends Neurosci 13:99–104.

Couey JJ, Meredith RM, Spijker S, Poorthuis RB, Smit AB, Brussaard AB, Mansvelder HD (2007) Distributed network actions by nicotine increase the threshold for spike-timing dependent plasticity in prefrontal cortex. Neuron 54:73–87.

Disney AA, Aoki C, Hawken MJ (2007) Gain modulation by nicotine in macaque V1. Neuron 56:701–713.

Disney AA, Aoki C, Hawken MJ (2012) Cholinergic suppression of visual responses in primate V1 is mediated by GABAergic inhibition. J Neurophysiol 108:1907–1923.

Drasdo A, Caulfield M, Bertrand S, Bertrand D, Wonnacott S (1992) Methyllycaconitine: a novel nicotinic antagonist. Mol Cell Neurosci 3:237–243.

Fenster CP, Rains MF, Noerager B, Quick MW, Lester RA (1997) Influence of subunit composition on desensitization of neuronal acetylcholine receptors at low concentrations of nicotine. J Neurosci 17:5747–5759.

Fenster CP, Beckman ML, Parker JC, Sheffield EB, Whitworth TL, Quick MW, Lester RA (1999) Regulation of α4β2 nicotinic receptor densitization by calcium and protein kinase C. Mol Pharmacol 55:432–443.

Fox AP, Nowycky MC, Tsien RW (1987) Kinetic and pharmacological properties distinguishing three types of calcium currents in chick sensory neurons. J Physiol (Lond.) 394:149–172.

Franklin KJB, Chudasama Y (2012) The prefrontal cortex. In: Watson C, Paxinos G, Puelles L, editors. The mouse nervous system. Amsterdam: Elsevier Academic Press. p. 727–735.

Fucile S (2004) Calcium permeability of nicotinic acetylcholine receptors. Cell Calcium 35:1–8.

Galarreta M, Hestrin S (2002) Electrical and chemical synapses among parvalbumin fast-spiking GABAergic interneurons in adult mouse neocortex. Proc Natl Acad Sci U S A 99:12438–12443.

Ghosh S, Reuveni I, Lamprecht R, Barkai E (2015) Persistent CaMKII activation mediates learning-induced long-lasting enhancement of synaptic inhibition. J Neurosci 25:128–139.

Griguoli M, Cherubini E (2012) Regulation of hippocampal inhibitory circuits by nicotinic acetylcholine receptors. J Physiol (Lond) 590:655–666.

Guillem K, Bloem B, Poorthuis RB, Loos M, Smit AB, Maskos U, Spijker S, Mansvelder HD (2011) Nicotinic acetylcholine receptor β2 subunits in the medial prefrontal cortex control attention. Science 333:888–891.

Gulledge AT, Park SB, Kawaguchi Y, Stuart GJ (2007) Heterogeneity of phasic cholinergic signaling in neocortical neurons. J Neurophysiol 97:2215–2229.

Harris KD, Mrsic-Flogel TD (2013) Cortical connectivity and sensory coding. Nature 503:51–58.

Harvey SC, Maddox FN, Luetje CW (1996) Multiple determinants of dihydro-beta-erythroidine sensitivity on rat neuronal nicotinic receptor alpha subunits. J Neurochem 67:1953–1959.

Isaacson JS, Scanziani M (2011) How inhibition shapes cortical activity. Neuron 72:231–243.

Ji D, Dani JA (2000) Inhibition and disinhibition of pyramidal neurons by activation of nicotinic receptors on hippocampal interneurons. J Neurophysiol 83:2682–2690.

Jiang X, Wang G, Lee AJ, Stornetta RL, Zhu JJ (2013) The organization of two new cortical interneuronal circuits. Nat Neurosci 16:210–218.

Jones BE (2008) Modulation of cortical activation and behavioral arousal by cholinergic and orexinergic systems. Ann N Y Acad Sci 1129:26–34.

Kargo WJ, Szatmary B, Nitz DA (2007) Adaptation of prefrontal cortical firing patterns and their fidelity to changes in action-reward contingencies. J Neurosci 27:3548–3559.

Kassam SM, Herman PM, Goodfellow NM, Alves NC, Lambe EK (2008) Developmental excitation of corticothalamic neurons by nicotinic acetylcholine receptors. J Neurosci 28:8756–8764.

Kawaguchi Y, Kondo S (2002) Parvalbumin, somatostatin and cholecystokinin as chemical markers for specific GABAergic interneuron types in the rat frontal cortex. J. Neurocytol. 31:277–287.

Kawaguchi Y (1993) Groupings of nonpyramidal and pyramidal cells with specific physiological and morphological characteristics in rat frontal cortex. J Neurophysiol 69:416–431.

Kepecs A, Fishell G (2014) Interneuron cell types are fit to function. Nature 505:318–326.

Klaassen A, Glykys J, Maguire J, Labarca C, Mody I, Boulter J (2006) Seizures and enhanced cortical GABAergic inhibition in two mouse models of human autosomal dominant nocturnal frontal lobe epilepsy. Proc Natl Acad Sci U S A 103:19152–19157.

Koliatsos VE, Martin LJ, Walker LC, Richardson RT, DeLong MR, Price DL (1988) Topographic, non-collateralized basal forebrain projections to amygdala, hippocampus, and anterior cingulated cortex in the rhesus monkey. Brain Res 463:133–139.

Lambe EK, Picciotto MR, Aghajanian GK (2003) Nicotine induces glutamate release from thalamocortical terminals in prefrontal cortex. Neuropsychopharmacology 28:216–225.

Le Magueresse C, Monyer H (2013) GABAergic interneurons shape the functional maturation of the cortex. Neuron 77:388–405.

Léna C, Changeux J-P (1997) Role of Ca^{2+} ions in nicotinic facilitation of GABA release in mouse thalamus. J Neurosci 17:576–585.

Lendvai B, Vizi ES (2008) Nonsynaptic chemical transmission through nicotinic acetylcholine receptors. Physiol Rev 88:333–349.

Letzkus JJ, Wolf SB, Meyer EM, Tovote P, Courtin J, Herry C, Lüthi A (2011) A disinhibitory microcircuit for associative fear learning in the auditory cortex. Nature 480:331–335.

Letzkus JJ, Wolff SB, Lüthi A (2015) Disinhibition, a circuit mechanism for associative learning and memory. Neuron 88:264–276.

McGarry LM, Packer AM, Fino E, Nikolenko V, Sippy T, Yuste R (2010) Quantitative classification of somatostatin-positive neocortical interneurons identifies three interneuron subtypes. Front Neural Circuits 4:12.

Mogg AJ, Jones FA, Pullar IA, Sharples CG, Wonnacott S (2004) Functional responses and subunit composition of presynaptic nicotinic receptor subtypes explored using the novel agonist 5-iodo-A-85380. Neuropharmacology 47:848–859.

Molas S, Dierssen M (2014) The role of nicotinic receptors in shaping and functioning of the glutamatergic system: a window into cognitive pathology. Neurosci Biobehav Rev 46:315–325.

Moser N, Mechawar N, Jones I, Gochberg-Sarver A, Orr-Urtreger A, Plomann M, Salas R, Molles B, Marubio L, Roth U, Maskos U, Winzer-Serhan U, Bourgeois JP, le Sourd AM, De Biasi M, Schröder H, Lindstrom J, Maelicke A, Changeux JP, Wevers A (2007) Evaluating the suitability of nicotinic acetylcholine receptor

antibodies for standard immunodetection procedures. J Neurochem 102:479–492.
Murphy BK, Miller KD (2009) Balanced amplification: a new mechanism of selective amplification of neural activity patterns. Neuron 61:635–648.
Murray TA, Bertrand D, Papke RL, George AA, Pantoja R, Srinivasan R, Liu Q, Wu J, Whiteaker P, Lester HA, Lukas RJ (2012) A7β2 Nicotinic acetylcholine receptors assemble, function, and are activated primarily via their α7-α7 interfaces. Mol Pharmacol 81:175–188.
Murray JD, Anticevic A, Gancsos M, Ichinose M, Corlett PR, Krystal JH, Wang X-J (2014) Linking microcircuit dysfunction to cognitive impairment: effects of disinhibition associated with schizophrenia in a cortical working memory model. Cereb Cortex 24:859–872.
Nutter TJ, Adams DJ (1995) Monovalent and divalent cation permeability and block of neuronal nicotinic receptor channels in rat parasympathetic ganglia. J Gen Physiol 105:701–723.
Okaty BW, Miller MN, Sugino K, Hempel CM, Nelson SB (2009) Transcriptional and electrophysiological maturation of neocortical fast-spiking GABAergic interneurons. J Neurosci 29:7040–7052.
Ozeki H, Finn IM, Schaffer ES, Miller KD, Ferster D (2009) Inhibitory stabilization of the cortical network underlies visual surround suppression. Neuron 62:578–592.
Palma E, Bertrand S, Binzoni T, Bertrand D (1996) Neuronal nicotinic α7 receptors expressed in Xenopus oocytes presents five putative binding sites for methyllycaconitine. J Physiol (Lond) 491:151–161.
Parikh V, Ji J, Decker MW, Sarter M (2010) Prefrontal β2 subunit-containing and α7 nicotinic acetylcholine receptors differentially control glutamatergic and cholinergic signaling. J Neurosci 30:3518–3530.
Paxinos G, Franklin KBJ (2001) The mouse brain in stereotaxic coordinates. 2nd ed. San Diego (CA): Academic Press. p. 296.
Paz JT, Huguenard JR (2015) Microcircuits and their interactions in epilepsy: is the focus out of focus? Nat Neurosci 18:351–359.
Pfeffer CK, Xue M, He M, Huang ZJ, Scanziani M (2013) Inhibition of inhibition in visual cortex: the logic of connections between molecularly distinct interneurons. Nat Neurosci 16:1068–1076.
Pi HJ, Hangya B, Kvitsiani D, Sanders JI, Huang ZJ, Kepecs A (2013) Cortical interneurons that specialize in disinhibitory control. Nature 503:521–524.
Picciotto MR, Highley MJ, Mineur YS (2012) Acetylcholine as a neuromodulator: cholinergic signaling shape nervous system function and behaviour. Neuron 76:116–129.
Poorthuis RB, Bloem B, Schak B, Wester J, de Kock CP, Mansvelder HD (2013) Layer-specific modulation of the prefrontal cortex by nicotinic acetylcholine receptors. Cereb Cortex 23:148–161.
Porter JT, Cauli B, Tsuzuki K, Lambolez B, Rossier J, Audinat E (1999) Selective excitation of subtypes of neocortical interneurons by nicotinic receptors. J Neurosci 19:5228–5235.
Price JL, Stern R (1983) Individual cells in the nucleus basalis-diagonal band complex have restricted axonal projections to the cerebral cortex in the rat. Brain Res 269:352–356.
Richardson KA, Fanselow EE, Connors BW (2008) Neocortical anatomy and physiology. In: Engel J, Pedley TA, editors. Epilepsy. A comprehensive textbook. Philadelphia: Lippincott Williams and Wilkins. p. 323–335.
Rudy B, Fishell G, Lee S, Hjerling-Leffler J (2011) Three groups of interneurons account for nearly 100% of neocortical GABAergic neurons. Dev Neurobiol 71:45–61.
Sarter M, Parikh V, Howe WM (2009) Phasic acetylcholine release and the volume transmission hypothesis: time to move on. Nat Rev Neurosci 10:383–390.
Shu Y, Hasenstaub A, McCormick D (2003) Turning on and off recurrent balanced cortical activity. Nature 423:288–293.
Sohal VS, Zhang F, Yizhar O, Deisseroth K (2009) Parvalbumin neurons and gamma rhythms enhance cortical circuit performance. Nature 459:698–702.
Tai C, Abe Y, Westenbroek RE, Scheuer T, Catterall WA (2014) Impaired excitability of somatostatin- and parvalbumin-expressing cortical interneurons in a mouse model of Dravet syndrome. Proc Natl Acad Sci U S A 111:E3139–E3148.
Tamás G, Buhl EH, Somogyi P (1997) Massive autaptic self-innervation of GABAergic neurons in cat visual cortex. J Neurosci 17:6352–6364.
Tsodyks MV, Skaggs WE, Sejnowski TJ, McNaughton BL (1997) Paradoxical effects of external modulation of inhibitory interneurons. J Neurosci 17:4382–4388.
Uylings HB, Groenewegen HJ, Kolb B (2003) Do rats have a prefrontal cortex? Behav Brain Res 146:3–17.
Walker LC, Kitt CA, DeLong MR, Price DL (1985) Noncollateral projections of basal forebrain neurons to frontal and parietal neocortex in primates. Brain Res Bull 15:307–314.
Wallace TL, Bertrand D (2013) Importance of the nicotinic acetylcholine receptor system in the prefrontal cortex. Biochem Pharmacol 85:1713–1720.
Walters CL, Cleck JN, Kuo YC, Blendy JA (2005) Mu-opioid receptor and CREB activation are required for nicotine reward. Neuron 46:933–943.
Wenger-Combremont AL, Bayer L, Dupré A, Mühlethaler M, Serafin M (2016) Slow bursting of mouse cortical layer 6b are depolarized by hypocretin/orexin and major transmitters of arousal. Front Neurol 7:88.
Xiang Z, Huguenard JR, Prince DA (1998) Cholinergic switching within neocortical inhibitory networks. Science 281:985–988.
Yang J-M, Zhang J, Yu Y-Q, Duan S, Li X-M (2014) Postnatal development of 2 microcircuits involving fast-spiking interneurons in the mouse prefrontal cortex. Cereb Cortex 24:98–109.
Zoli M, Pistillo F, Gotti C (2015) Diversity of native nicotinic receptor subtypes in mammalian brain. Neuropharmacology 96:302–311.
Zolles G, Wagner E, Lampert A, Sutor B (2009) Functional expression of nicotinic acetylcholine receptors in rat neocortical layer 5 pyramidal cells. Cereb Cortex 19:1079–1091.
Zwart R, Vijverberg HP (1997) Potentiation and inhibition of neuronal nicotinic receptors by atropine: competitive and noncompetitive effects. Mol Pharmacol 52:886–895.
Zwart R, Broad LM, Xi Q, Lee M, Moroni M, Bermudez I, Sher E (2006) 5-I-A-85380 and TC-2559 differentially activate heterologously expressed α4β2 nicotinic receptors. Eur J Pharmacol 539:10–17.

(Accepted 18 October 2016)
(Available online 26 October 2016)